RSC Advances

ROYAL SOCIETY OF CHEMISTRY

PAPER

View Article Online
View Journal | View Issue

Check for updates

Cite this: *RSC Adv.*, 2020, **10**, 36371

The fabrication and characterization of CeO_2/Cu_2O nanocomposites with enhanced visible-light photocatalytic activity

Zheng Dong,[a] Bo Yang,[b] Haibo Chang *[a] and Li Li*[a]

Received 21st July 2020
Accepted 14th September 2020

DOI: 10.1039/d0ra06345b

rsc.li/rsc-advances

Spherical Cu_2O nanocrystals were synthesized and CeO_2/Cu_2O nanocomposites were successfully prepared from the spherical Cu_2O nanocrystals. Characterization analysis was performed *via* scanning electron microscope (SEM), transmission electron microscope (TEM), X-ray diffraction (XRD), X-ray photoelectron spectroscopy (XPS), and UV-visible diffusion reflectance spectroscopy (DRS) studies. In comparison with the Cu_2O nanocrystals, the CeO_2/Cu_2O nanocomposites exhibited high visible-light-induced photocatalytic activity for the degradation of methyl orange solution. Radical trapping experiments proved that photo-generated electrons played a very minor role, while photo-generated holes and superoxide radicals played a major role in the degradation process. The CeO_2/Cu_2O system could cause the internal energy band to bend, leading to the building of internal electric fields. The excited electrons and holes easily moved in opposite directions, promoting the effective separation of charges, which obviously enhanced the visible light photocatalytic activity of the catalyst.

Introduction

Nowadays, environmental pollution has become a severe problem which restricts economic development and affects the health of human beings.[1–4] Every year, more than 70 thousand tons of chemical dyes are produced with widespread applications in industries around the world.[5,6] Methyl orange (MO) is one of these, which is used in the chemical, medical and dyeing industries.[7] Treating dye wastewaters is a crucial worldwide problem and it is attracting researchers' attention.

Environmentally friendly semiconductor catalysts have been used a lot in research and commerce.[8–10] Cuprous oxide (Cu_2O) is a narrow band-gap semiconductor (2.17 eV), absorbing 42% of solar energy.[11] Cu_2O exhibits advantages over other semiconductors due to its low toxicity, better environmental acceptability and resource reserve rate.[12] However, the photocatalytic activity of pure Cu_2O is restricted due to its low hole mobility and utilization rate. Researchers have tried to promote charge separation, interfacial charge transfer and to extend the life of the carriers to enhance the catalyst's capacity by doping elements[13–15] or combining precious metals,[16] other semiconductors and carbon materials.[17–19] Ceria (CeO_2) is a superior semiconductor material with a band gap of 3.2 eV. Ceria is broadly applied in many fields because of its high oxygen storage capacity and stabilization.[20] Under light excitation, the tetravalent ions can not only effectively inhibit the simple recombination of electrons and holes, leading to enhanced photocatalytic efficiency, but also red-shifts the light absorption wavelength to the visible-light region, which increases the effective utilization of solar energy.[21,22] Lou *et al.*[23] obtained CuO/CeO_2 by an impregnation method, and it exhibited high catalytic activity in pollution oxidation. The researchers reported that deposition of CeO_2 by other oxides led to a stronger redox property and high catalytic activity attributed to the formation of interfacial active centers between CeO_2 and oxide.[24] On the other hand, nanoscale crystals of CeO_2 generally exhibit higher interfacial density, which generates a large number of carriers to promote oxidizability.[25]

In this study, we have successfully synthesized spherical Cu_2O nanocrystals and deposited CeO_2 nanoparticles on their surface. The photocatalytic activity of the catalyst composites is measured by the degradation of MO solution under visible light. The photocatalytic mechanism is discussed.

Experimental

Materials

All chemical reagents used in this experiment were of analytical grade and purchased from Sinopharm Chemical Reagent Co., Ltd, including cupric acetate anhydrous [$Cu(Ac)_2$], hydrazine hydrate ($N_2H_4 \cdot H_2O$), cerium nitrate hexahydrate [$Ce(NO_3)_3 \cdot 6H_2O$], ethyl alcohol (C_2H_5OH), sodium hydroxide (NaOH), methyl orange (MO), isopropanol (IPA), triethanolamine (TEA), benzoquinone (BQ) and sulfamethoxazole (SMX). Deionized water was obtained from centrally prepared water.

---

[a] *College of Resource and Environmental Science, Jilin Agricultural University, Changchun 130118, China. E-mail: changhb@jlau.edu.cn; Fax: +86-431-84532955*

[b] *Taonan Comprehensive Experimental Station, Jilin Academy of Agricultural Sciences, Taonan 137100, China*

Sample preparation

To synthesize Cu_2O nanocrystals, 1 g of $Cu(Ac)_2$ was mixed with 20 ml of deionized water and stirred to complete dissolution, presenting a blue solution at room temperature, and then 30 ml of IPA was added into the solution. The solution was kept in a water bath at 84 °C for 10 minutes. 5 ml of 1 M $N_2H_4 \cdot H_2O$ was added in a dropwise manner. After 10 min, brick-red Cu_2O was obtained. The Cu_2O nanocrystals were modified by a later procedure. Different concentrations of $Ce(NO_3)_3 \cdot 6H_2O$ solution (0.625 mM, 1.25 mM, 2.5 mM and 5 mM) were respectively mixed with Cu_2O nanocrystals and kept in a water bath at 84 °C. Finally, NaOH solution was added. The collected CeO_2/Cu_2O nanocomposites were centrifuged and washed with deionized water and ethyl alcohol, and finally dried at 60 °C for 12 h.

Characterization

The crystal structure and properties of the samples were studied by X-ray diffraction (XRD-7000, Shimadzu Corporation, Japan), using copper Kα ($\lambda = 0.15418$ nm) as the radiation source, and the scanning range was from 20 to 80°. A scanning electron microscope (SSX-550, Shimadzu Corporation, Japan) and a transmission electron microscope (Tecnai F20, FEI) were used to observe the surface morphology of the samples. X-ray photoelectron spectroscopy was performed on a VG ESCALAB LKII instrument with an Mg-Kα-ADES ($h\nu = 1253.6$ eV) source and the residual gas pressure was below 1028 Pa. Total organic carbon (TOC) analysis was conducted with a TOC/TNb Analyzer (Multi N/C 2100, Analytik Jena, Germany). The SMX photocatalytic degradation was determined using a liquid chromatograph (HPLC) system (Agilent Technologies, 1290 Infinity II). Chromatographic separation was performed using a C18 chromatographic column (5 μm, 250 mm × 3.5 mm) with an injection volume of 50 μl at a flow rate of 1 ml min^{-1}. The composition of the mobile phase was 30% methanol and 70% pure water and the pH was adjusted to 3.5 using formic acid. A diffuse reflection UV-visible spectrophotometer (TU-1950, Beijing Purkinje General) was used to evaluate the optical properties of the samples. A UV-visible spectrophotometer (TU-1950, Beijing Purkinje General) was used to measure the absorbance of MO.

Photocatalytic activity experiments

The samples (20 mg) were added to a quartz beaker containing 30 ml of 10 mg l^{-1} MO solution, and stirred for 30 minutes in the dark. The samples were uniformly dispersed in the MO solution and reached adsorption–desorption equilibrium. In order to determine the concentration of MO solution, the MO solution (3 ml) was taken out and centrifuged, and the absorbance was measured with an ultraviolet spectrophotometer, which was recorded as A_0. After that, the solution was stirred in a photoreactor and illuminated with a 300 W xenon lamp equipped with a UV-cutoff-filter to provide a visible-light source with ≥400 nm. 3 ml of MO solution were taken out every 30 minutes after visible-light irradiation, and then centrifuged at 8000 rpm for 10 minutes. The supernatant was collected and returned to the quartz beaker. Recycling experiments and TOC experiments were performed by the same process.

SMX was selected as the other target compound to further evaluate the photocatalytic activity of CeO_2/Cu_2O nanocomposites under visible-light irradiation. The concentration of SMX solution was 20 mg l^{-1} in the photodegradation experiment. The degradation process was the same as for the degradation of MO.

The photocatalytic degradation efficiency (%) was calculated with the following formula:

$$\text{Degradation (\%)} = (C_0 - C)/C_0 \times 100\%$$

where C is the concentration of the MO solution at time t, and C_0 is the adsorption–desorption equilibrium concentration of MO.

In the experiment for SMX photodegradation, the calculation method was the same as that for MO degradation.

Additionally, the radical trapping experiments were the same as that for MO solution. After reaching adsorption–desorption equilibrium, IPA, TEA, and BQ were added to the solution as capture agents for hydroxyl radicals, holes, and superoxide radicals to study the activities in the photocatalytic reaction.

Results and discussion

Characterization of samples

In the following degradation experiment, the CeO_2/Cu_2O nanocomposites prepared by 1.25 mM $Ce(NO_3)_3 \cdot 6H_2O$ solution were chosen for characterization. The morphological features of Cu_2O nanocrystals and CeO_2/Cu_2O nanocomposites were investigated by SEM, TEM and HRTEM. The Cu_2O nanocrystals are spherical with a diameter of about 550 nm, and the surface of the Cu_2O nanocrystals is slightly rough (Fig. 1a and b). When the CeO_2 nanoparticles are loaded on their surface, the $CeO_2/$

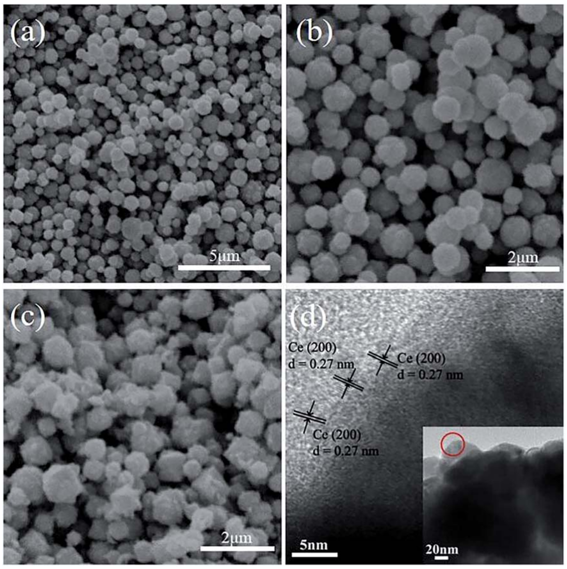

Fig. 1 SEM images of (a and b) Cu_2O and (c) CeO_2/Cu_2O. (d) A TEM image of CeO_2/Cu_2O.

Cu_2O nanocomposites appear to have irregular shapes (Fig. 1c). The HRTEM image of the selected areas was measured and is shown in the insets to Fig. 1d. The spacing of adjacent lattice planes is *ca.* 0.27 nm, which can be ascribed to the interplanar spacing of the (200) plane of the CeO_2 nanoparticles. The inset shows the corresponding TEM images of the CeO_2/Cu_2O nanocomposites.

The XRD patterns of Cu_2O nanocrystals, CeO_2 nanoparticles and CeO_2/Cu_2O nanocomposites are presented in Fig. 2. The diffraction peaks can be indexed to Cu_2O (JCPDS no. 34-1354) and CeO_2 (JCPDS no. 43-1002). The diffraction peaks appear at the positions about 29.7°, 36.5°, 42.5°, 61.5°, and 73.6°, corresponding to (110), (111), (200), (220) and (311) of Cu_2O nanocrystals. No other characteristic impurity peaks are detected in the Ce_2O nanoparticles (Fig. 2a). The diffraction peaks of the CeO_2/Cu_2O nanocomposites are strong and narrow, which indicates that the composites are highly crystalline (Fig. 2b). CeO_2 nanoparticles are deposited on the surface of the Cu_2O nanocrystals.

However, the diffraction peaks of the CeO_2 nanoparticles do not appear in Fig. 2c due to the small amount of CeO_2 nanoparticles on the surface of the Cu_2O nanocrystals which is below the detection limit of XRD analysis.

X-ray photoelectron spectroscopy is used to determine the surface elemental composition and chemical state of the Cu_2O nanocrystals and CeO_2 nanoparticles. The C, Cu, Ce, and O peak regions of the CeO_2/Cu_2O nanocomposites can be clearly seen (Fig. 3a). The C 1s peak at 284.4 eV is used as a reference peak for calibration of all the spectra. The peaks at 932.1 eV and 951.9 eV are characteristic peaks of Cu $2p_{3/2}$ and Cu $2p_{1/2}$, respectively (Fig. 3b). The positions of the peaks are consistent with cuprous oxide. The peak of the CeO_2/Cu_2O nanocomposites obviously shifts in the direction of high binding energy compared with that of the Cu_2O nanocrystals. The difference between the two peaks is 8.1 eV from the binding energy, which indicates that there is an electronic exchange between Cu_2O and CeO_2,[26] and also proves that CeO_2 nanoparticles are successfully deposited on the surface of the Cu_2O nanocrystals. Two peaks at 905.0 eV and 886.6 eV appear in the Ce 3d spectrum, corresponding to the binding energies of Ce $3d_{3/2}$ and Ce $3d_{5/2}$, respectively (Fig. 3c). The peak located at the binding energy of 531.7 eV is contributed by the O 1s of the CeO_2/Cu_2O nanocomposites (Fig. 3d).

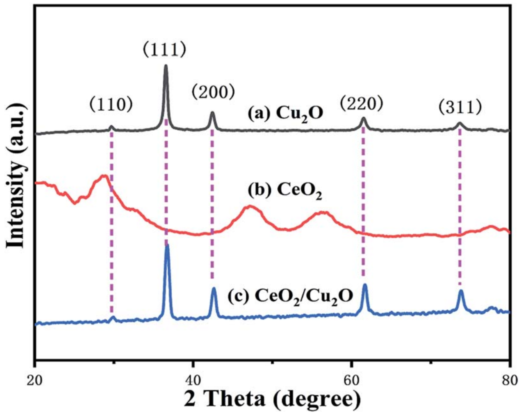

Fig. 2 XRD patterns of (a) Cu_2O, (b) CeO_2, and (c) CeO_2/Cu_2O.

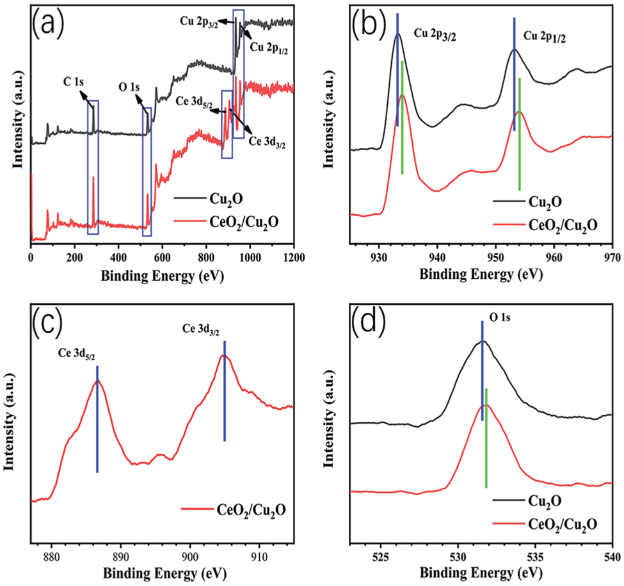

Fig. 3 Survey-scan XPS spectra of Cu_2O and CeO_2/Cu_2O (a), and Cu 2p (b), Ce 3d (c), and O 1s (d) spectra.

To investigate the optical properties of the samples, Cu_2O nanoparticles and CeO_2/Cu_2O nanocomposites were analyzed with diffuse reflectance spectra. Clearly, Cu_2O nanocrystals display weak absorption in the range 450–600 nm (Fig. 4a). Compared with Cu_2O nanocrystals, an evident red shift is observed for the CeO_2/Cu_2O nanocomposites. They exhibit strong absorption in the region from 550 to 650 nm (Fig. 4a), which shows a significant extension in the absorption of light. The optical band gap of the samples is calculated from following formula: $(Ah\nu)^2 = h\nu - E_g$, where A, h, ν and E_g are the absorption coefficient, Planck's constant, incident photon frequency and band gap, respectively.[27] The band gap of the Cu_2O nanocrystals is 2.28 eV, and that of the CeO_2/Cu_2O composites is extrapolated to be 2.06 eV, which indicates that depositing CeO_2 nanoparticles on the surface of Cu_2O nanocrystals could narrow the band gap of the catalysts (Fig. 4b).

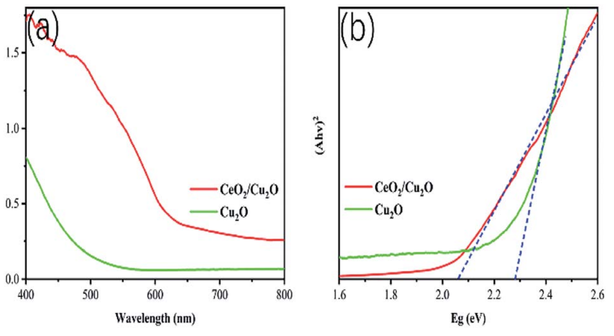

Fig. 4 (a) UV-vis DRS spectra for Cu_2O and CeO_2/Cu_2O. (b) Band gaps of the photocatalysts.

This is beneficial for enhancing the photocatalytic activity of the composite which is identified by subsequent studies.

Organic dyes are extensively applied in industrial production, causing the emergence of environmental issues and affecting human health.[28,29] Therefore, MO solution was chosen as the simulated pollutant to evaluate the photocatalyst activity. The photodegradation properties of the samples for an MO solution were measured. The adsorption experiment was firstly performed for 30 minutes in the dark to reach adsorption–desorption equilibrium, eliminating the influence of physical adsorption. In order to explore the effects of different amounts of CeO_2 nanoparticles, parallel experiments were performed with different concentrations of $Ce(NO_3)_3 \cdot 6H_2O$ solution, and the results are shown in Fig. 5. The Cu_2O nanocrystals present a photocatalytic activity with 61.88% of the MO solution degraded after irradiation for 2.5 h. The photocatalytic activity is dramatically enhanced after CeO_2 nanoparticles are loaded on the surface of the Cu_2O nanocrystals. When the concentrations of $Ce(NO_3)_3 \cdot 6H_2O$ solution are 5 mM and 2.25 mM, the degradation of the MO solution increases with a further decrease in the concentration of $Ce(NO_3)_3 \cdot 6H_2O$ solution. Among the photocatalysts, the highest photocatalytic activity is 85.11% with 1.25 mM $Ce(NO_3)_3 \cdot 6H_2O$ solution. The degradation rate of MO solution increases, which is mainly caused by the deposition of CeO_2 nanoparticles. The electrons generated by the visible-light excitation of Cu_2O nanocrystals will transfer to CeO_2 nanoparticles, which is conducive to the conduction of electrons and separation of electrons and holes. However, the photocatalytic activity declines slightly (83.74%) when the concentration of the $Ce(NO_3)_3 \cdot 6H_2O$ solution is 0.625 mM.

The mineralization ratio for the decomposition of MO solution on the CeO_2/Cu_2O composite photocatalyst prepared with 1.25 mM $Ce(NO_3)_3 \cdot 6H_2O$ solution was evaluated by TOC analysis. The removal rate of TOC is approximately 68.98% after 2.5 h (Fig. 6). This indicates that plenty of MO is noticeably mineralized by the CeO_2/Cu_2O composite photocatalyst.

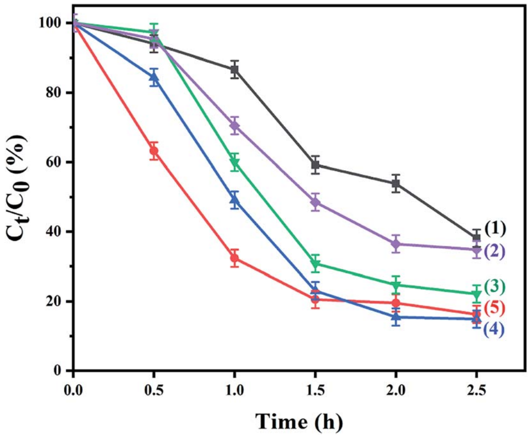

Fig. 5 The relationship between C_t/C_0 and irradiation time (t) in the photodegradation of MO solution. (1) Cu_2O and (2–5) CeO_2/Cu_2O in the presence of $Ce(NO_3)_3 \cdot 6H_2O$ solution: (2) 5 mM, (3) 2.5 mM, (4) 1.25 mM, and (5) 0.625 mM.

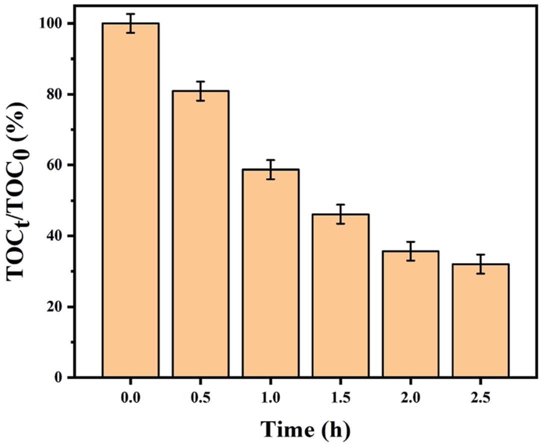

Fig. 6 The removal of TOC with the CeO_2/Cu_2O nanocomposite photocatalyst.

Additionally, the temporal variation in absorption spectra of MO solution under visible-light irradiation is demonstrated, in which it is obviously observed that the degradation rate for MO solution of CeO_2/Cu_2O nanocomposites is much higher than that of Cu_2O nanocrystals (Fig. 7).

The stability of the photocatalyst is important for its application. A cycling experiment was performed and shown in Fig. 8a. The degradation rate of the MO solution is only gradually reduced, and it remains at 70% after 4 repeated experiments. After each cycle, the photocatalysts are collected by centrifugation, washed with deionized water, and then dried in a vacuum for 10 h. A slight deactivation of the photocatalyst is detected after 4 cycles attributed to a reduction in the minority of the photocatalyst when it is centrifuged, washed, and dried. The excellent performance of the CeO_2/Cu_2O nanocomposites decreases the cost and environmental burden for applications in pollutant degradation.

The XRD patterns of fresh and 4-times-used CeO_2/Cu_2O nanocomposites are shown in Fig. 8b. It can be seen that the phase and structure of the CeO_2/Cu_2O nanocomposites have not obviously changed after 4 times, suggesting that the photocatalyst is stable during the reaction.

The colorless pollutant antibiotic SMX was chosen as a different type of model pollutant to assess photocatalytic

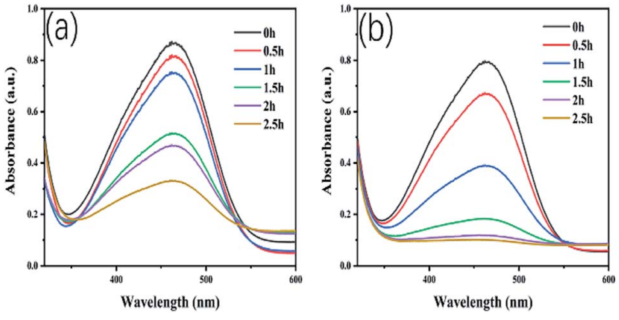

Fig. 7 Change in absorption spectra of MO under visible light irradiation for Cu_2O (a) and (b) CeO_2/Cu_2O.

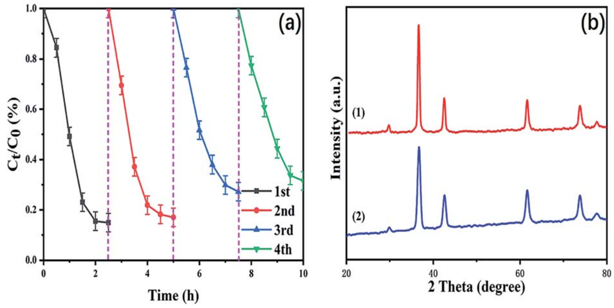

Fig. 8 (a) Recycling tests for MO solution photodegradation in the presence of CeO_2/Cu_2O samples under visible-light irradiation. (b) The XRD patterns of CeO_2/Cu_2O nanocomposites: (1) fresh and (2) after 4 photocatalytic experiment cycles.

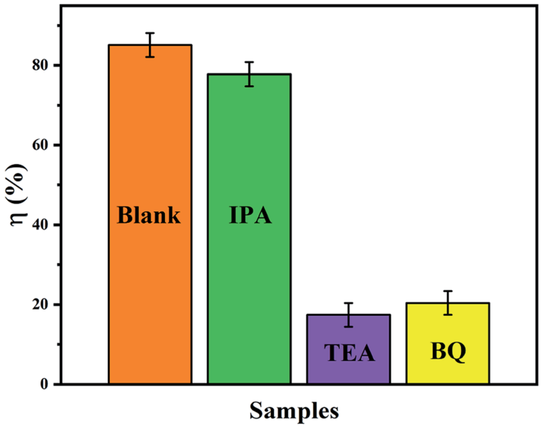

Fig. 10 Photocatalytic degradation efficiency of MO solution over CeO_2/Cu_2O nanocomposites: blank, and in the presence of IPA, TEA, and BQ.

activity of the CeO_2/Cu_2O nanocomposites, which were synthesized with 1.25 mM $Ce(NO_3)_3 \cdot 6H_2O$ solution. The SMX solution is degraded significantly with a degradation ratio of 89.80% within the first 30 minutes under visible-light irradiation. In the following 2 h, the removal efficiency of SMX tended to level off and reached 91.95% at 2.5 h (Fig. 9). The experimental results indicate that the CeO_2/Cu_2O nanocomposites appear to have remarkable degradation activity for SMX and may become a useful photocatalytic composite for potential applications in environmental management.

In order to study the role of each active species in the catalytic process, the following of comparative experiments were carried out; see Fig. 10. To each group of MO solutions were added IPA, TEA and BQ to capture the hydroxyl radicals ($OH^{\bullet}$), the photo-generated holes (h^+) and the superoxide radicals ($\cdot O^{2-}$), respectively.[30] After adding IPA to the MO solution, the photocatalytic efficiency (η%) of the CeO_2/Cu_2O nanocomposites decreased weakly, which shows that $OH^{\bullet}$ is not the principal factor for MO solution degradation in this process. However, the degradation rate of the photocatalyst decreased remarkably in the presence of TEA and BQ compared with that of blank, which indicates that the TEA consumes the photo-generated holes generated in the system and reduces the reaction with MO solution. Furthermore, BQ removes oxygen dissolved in water, decreasing the amount of oxygen adsorbed on the surface of the catalyst and its interaction with photo-generated electrons. The degradation rate of MO solution decreases due to the lower number of superoxide radicals. This proves that h^+ and $\cdot O^{2-}$ play crucial roles in the photocatalytic degradation of MO solution.[31]

The photocatalytic mechanism is concluded according to the above information (Fig. 11.). The difference in chemical potential between Cu_2O nanocrystals and CeO_2 nanoparticles causes band bending at the junction interface. The bending of the energy band leads to the building of an internal electric field promoting photo-excited electrons and holes to move in opposite directions.[32] The charges are effectively separated which outstandingly enhances the photocatalytic activity under visible-light irradiation.[33,34] When the electrons on the valence band of the CeO_2 nanoparticles are excited, some of the electrons jump to the conduction band of the CeO_2 nanoparticles and the valence band of the Cu_2O nanocrystals. Holes are formed. The excited electrons become photo-generated electrons. Similarly, the electrons on the valence band of the Cu_2O

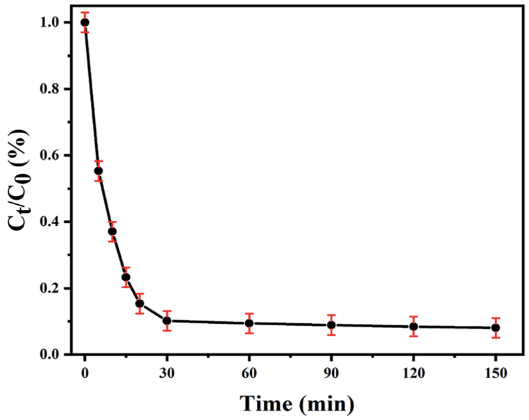

Fig. 9 Photocatalytic rate of SMX solution degradation using CeO_2/Cu_2O nanocomposites under visible-light irradiation.

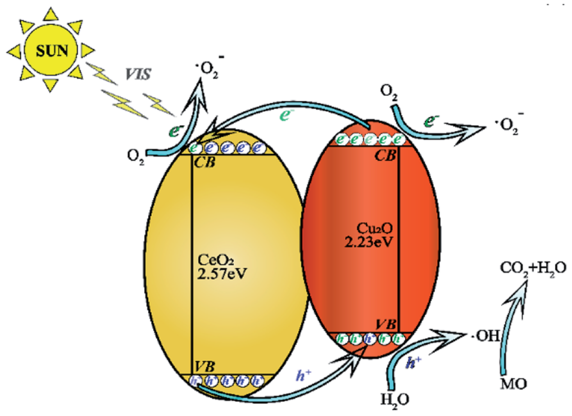

Fig. 11 The CeO_2/Cu_2O nanocomposite degradation mechanism.

nanocrystals are excited to form photo-generated electrons with negative charge. Some of them cooperatively transfer to the valence band of the CeO_2 nanoparticles and the others react with O_2 creating $\cdot O^{2-}$. The photo-generated holes are left on the surface of the valence band on the Cu_2O nanocrystals which react with external H_2O to form $\cdot OH$, and a small part of the $\cdot O^{2-}$ are adsorbed by the holes on the catalyst surface to generate $\cdot HO_2$.[35] These active radicals formed can break the strong azo bonds of the MO solution, and finally degrade them into non-toxic and harmless CO_2 and H_2O. The degradation process is shown by following formulas.

$$CeO_2/Cu_2O + h\nu \rightarrow Cu_2O(e_{CB}^-) + CeO_2(e_{CB}^-) + Cu_2O(h_{VB}^+) + CeO_2(h_{VB}^+) \quad (1)$$

$$Cu_2O(e_{CB}^-) + O_2 \rightarrow Cu_2O + \cdot O_2^- \quad (2)$$

$$CeO_2(e_{CB}^-) + O_2 \rightarrow CeO_2 + \cdot O_2^- \quad (3)$$

$$Cu_2O(h_{VB}^+) + OH^- \rightarrow Cu_2O + \cdot HO \quad (4)$$

$$CeO_2(h_{VB}^+) + OH^- \rightarrow CeO_2 + \cdot HO \quad (5)$$

$$\cdot O_2^- + H^+ \rightarrow \cdot HO_2 \quad (6)$$

$$MO + \cdot HO_2 \rightarrow CO_2 + H_2O \quad (7)$$

Conclusions

In summary, we prepared spherically structured Cu_2O nanocrystals and successfully loaded CeO_2 nanoparticles onto the surfaces of the Cu_2O nanocrystals *via* a precipitation method. When the concentration of $Ce(NO_3)_3 \cdot 6H_2O$ solution is 0.25 mM, the CeO_2/Cu_2O nanocomposites exhibit an optimal catalytic effect. The degradation rate of MO solution increased by 23.23% compared with that when using Cu_2O nanocrystals (61.88%), showing a significant improvement in the degradation efficiency of Cu_2O nanocrystals. Photo-generated holes and superoxide radicals play crucial roles in the process of degradation of MO solution. CeO_2/Cu_2O nanocomposites still maintained excellent catalytic activity after 4 repeat cycles, demonstrating that the CeO_2/Cu_2O nanocomposite was a potential visible-light photocatalyst. This research will provide deeper insights into the use of CeO_2/Cu_2O nanocomposites to treat industrial dye wastewater.

Conflicts of interest

The authors declare no conflicts of interest.

Acknowledgements

This work was supported by the Science and Technology Department of Jilin Province ((20190303086SF) and (20200201011JC)).

Notes and references

1 L. F. Yang, J. B. Liu, H. B. Chang and S. S. Tang, *RSC Adv.*, 2015, **5**, 59970.
2 J. Ren, W. Wang, S. Sun, L. Zhang, L. Wang and J. Chang, *Ind. Eng. Chem. Res.*, 2011, **50**, 10366.
3 M. G. Alalm, A. Tawfik and S. Ookawara, *J. Environ. Chem. Eng.*, 2016, **4**, 1929.
4 M. X. Zhang, J. He, Y. B. Chen, P. Y. Liao, Z. Q. Liu and M. S. Zhu, *Chin. Chem. Lett.*, 2020, DOI: 10.1016/j.cclet.2020.05.001.
5 T. H. Tran, A. H. Le, T. H. Pham, D. T. Nguyen and S. W. Chang, *Sci. Total Environ.*, 2020, **725**, 138325.
6 H. Pang, F. Gao and Q. Lu, *Chem. Commun.*, 2009, 1076.
7 M. Jung, J. N. Hart, J. Scott, Y. H. Ng, Y. Jiang and R. Amal, *Appl. Catal., A*, 2016, **521**, 190.
8 W. Y. Ching, Y. N. Xu and K. W. Wong, *Phys. Rev. B: Condens. Matter*, 1989, **40**, 7684.
9 M. S. Zhu, C. Y. Zhai, S. Kim, M. Fujitsuka and T. Majima, *J. Phys. Chem. Lett.*, 2019, **10**, 4017.
10 H. M. Zhang, J. He, C. Y. Zhai and M. S. Zhu, *Chin. Chem. Lett.*, 2019, **30**, 2338.
11 M. Zayat, P. G. Parejo and D. Levy, *Chem. Soc. Rev.*, 2007, **36**, 1270.
12 A. K. Mishra and D. Pradhan, *Cryst. Growth Des.*, 2016, **16**, 3688.
13 X. Han, X. He, F. Wang, J. Chen, J. Xu, X. Wang and X. Han, *J. Mater. Chem. A*, 2017, **5**, 10220.
14 M. Zou, H. Liu, L. Feng, T. Thomas and M. Yang, *Solid State Sci.*, 2017, **65**, 22.
15 F. Ye, J. J. Zeng, X. M. Cai, X. Q. Su, B. Wang, H. Wang, V. A. L. Roy, X. Q. Tian, J. W. Li, D. P. Zhang, P. Fan and J. Zhang, *J. Alloys Compd.*, 2017, **721**, 64.
16 X. W. Liu, *Langmuir*, 2011, **27**, 9100.
17 Y. Ghayeb, M. M. Momeni and M. Menati, *J. Mater. Sci.: Mater. Electron.*, 2017, **28**, 7650.
18 A. A. Dubale, W. N. Su, A. G. Tamirat, C. J. Pan, B. A. Aragaw, H. M. Chen, C. H. Chen and B. J. Hwang, *J. Mater. Chem. A*, 2014, **2**, 18383.
19 J. Ma, N. Jia, C. Shen, W. Liu and Y. Wen, *J. Hazard. Mater.*, 2019, **378**, 120782.
20 P. Aunbamrung and A. Wongkaew, *Adv. Chem. Eng. Sci.*, 2013, **3**, 15.
21 Y. Lee, G. He, A. J. Akey, R. Si, M. F. Stephanopoulos and I. P. Herman, *J. Am. Chem. Soc.*, 2011, **133**, 12952.
22 S. Dey and G. C. Dhal, *Mater. Sci. Energy Technol.*, 2020, **3**, 6.
23 M. F. Lou, Y. J. Zhong, X. X. Yuan and X. M. Zheng, *Appl. Catal., A*, 1997, **162**, 121.
24 D. Nickolova, E. Stoyanova, D. Stoychev, I. Avramova and P. Stefanov, *Surf. Coat. Technol.*, 2008, **202**, 1876.
25 H. Du, Y. N. Liu, C. C. Shen and A. W. Xu, *Chin. J. Catal.*, 2017, **38**, 1295.
26 J. J. Wang, G. N. Li and Z. l. Li, *Sci. Adv.*, 2017, **3**, 1701290.
27 K. Lalitha, G. Sadanandam, V. D. Kumari, M. Subrahmanyam, B. Sreedhar and N. Y. Hebalkar, *Phys. Chem. Chem. Phys.*, 2010, **114**, 22181.

28 X. Hu, X. Zhou, R. Wang, C. Hu and J. Qu, *Appl. Catal., B*, 2014, **154–155**, 44.

29 V. K. Mrunal, A. K. Vishnu, N. Momin and J. Manjanna, *Environ. Nanotechnol. Monit. Manag.*, 2019, **12**, 100265.

30 P. Zhou, J. Yu and M. Jaroniec, *Adv. Mater.*, 2014, **26**, 4920.

31 T. Arai, M. Yanagida, Y. Konishi, Y. Iwasaki and H. Sugihara, *J. Phys. Chem. C*, 2007, **111**, 7574.

32 J. C. Wang, S. L. Lou, Y. Li, Y. W. Fang and Y. Y. Ren, *ACS Appl. Mater. Interfaces*, 2015, **7**, 8631.

33 H. Du, Y. N. Liu, C. C. Shen and A. W. Xu, *Chin. J. Catal.*, 2017, **38**, 1295.

34 L. Wang, Y. Li, P. F. Han and Y. X. Jiang, *RSC Adv.*, 2020, **10**, 22432.

35 J. Jin, W. Song, N. Zhang, L. J. Li, H. Hao, B. Yang and B. Zhao, *RSC Adv.*, 2020, **10**, 26639.